NANO LETTERS

pubs.acs.org/NanoLett

Performance of Ultrathin Silicon Solar Microcells with Nanostructures of Relief Formed by Soft Imprint Lithography for Broad Band Absorption Enhancement

Dan Shir,[†,||] Jongseung Yoon,[†,||] Debashis Chanda,[†] Jae-Ha Ryu,[†] and John A. Rogers*[,†,‡,§]

[†] Departments of Materials Science and Engineering, Beckman Institute, and Frederick Seitz Materials Research Laboratory, University of Illinois at Urbana−Champaign, 1304 West Green Street, Urbana, Illinois 61801, [‡] Department of Chemistry, University of Illinois at Urbana−Champaign, Urbana, Illinois 61801, and [§] Department of Electrical and Computer Engineering, Mechanical Science and Engineering, University of Illinois at Urbana−Champaign, 1304 West Green Street, Urbana, Illinois 61801

ABSTRACT Recently developed classes of monocrystalline silicon solar microcells can be assembled into modules with characteristics (i.e., mechanically flexible forms, compact concentrator designs, and high-voltage outputs) that would be impossible to achieve using conventional, wafer-based approaches. This paper presents experimental and computational studies of the optics of light absorption in ultrathin microcells that include nanoscale features of relief on their surfaces, formed by soft imprint lithography. Measurements on working devices with designs optimized for broad band trapping of incident light indicate good efficiencies in energy production even at thicknesses of just a few micrometers. These outcomes are relevant not only to the microcell technology described here but also to other photovoltaic systems that benefit from thin construction and efficient materials utilization.

KEYWORDS Nanoimprint lithography, soft lithography, optical nanostructures, photovoltaics, silicon, light trapping

Photovoltaic (PV) technologies can play important roles in satisfying future demands for energy. As an active material, silicon retains a dominant position in PV due to its high natural abundance, good properties, and reliability in solar cells and to the existence of a mature, established infrastructure for its production.[1] Research in this area has the potential to enable advances through designs that provide new capabilities or increased performance or through methods that reduce the cost by improving the utilization of the materials. Solar cells based on thin films of amorphous or polycrystalline silicon require substantially less material compared to bulk wafer-based systems and, in certain cases, they can be used in mechanically flexible layouts. The efficiencies, on the other hand, are poor compared to those achievable with monocrystalline silicon. Several emerging strategies exist for using this form of silicon in ways that offer design possibilities and performance that cannot be achieved in traditional wafer geometries. One example exploits miniature spherical cells with diameters of ~1 mm formed from molten droplets of silicon.[2] In other work, micromachining through the thicknesses of silicon wafers yields thin (~50 μm) "slivers" of silicon oriented on edge relative to the wafer surfaces. Rotating these elements by 90°, mechanical manipulating them into ordered arrays, and then electrically interconnecting them yields an interesting type of module with many attractive characteristics.[3] We recently reported an approach[4] that exploits near-surface etching of ⟨111⟩ wafers using methods originally developed for applications in flexible electronics[5,6] to yield ultrathin (down to micrometers) cells in the form of microscale bars and ribbons (i.e., microcells). Techniques of transfer printing provide versatile routes for high throughput, massively parallel assembly of such cells into modules; interconnection using planar processing methods or direct write printing[7] completes the fabrication. These designs enable efficient use of silicon, in formats that offer high performance together with other potentially attractive features such as lightweight, mechanically flexible construction,[4] high voltage outputs,[4,8] and easy integration with microlenses for low profile concentrator layouts[4] or with sparse cell coverages for partially transparent configurations.[4] The thickness (~15 μm) of silicon needed to achieve good energy conversion efficiencies (i.e., ~12% with backside reflectors, but otherwise unoptimized designs[4]) is roughly 10 times less than that used in conventional systems. Reducing the thickness even further is of interest to decrease the consumption of silicon and to enhance other module features, such as mechanical flexibility and radiation hardness, that depend critically on thin geometries. A key challenge is that, although the fabrication and printing schemes are compatible with

* To whom correspondence should be addressed, jrogers@uiuc.edu.

[||] Authors contributed equally.

Received for review: 4/29/2010
Published on Web: 06/28/2010

extremely thin designs, the efficiencies decrease steeply for thicknesses below ~15 μm due to incomplete optical absorption.[4]

This apparent limitation can be avoided by increasing the optical interaction length through diffraction and/or scattering. Statistical ray-tracing techniques suggest that this length can be increased by up to ~25 times for completely randomized light and weakly absorbing materials with backside reflectors.[9] Surfaces that provide randomization, however, can be difficult to achieve.[9] A common approach for texturing monocrystalline silicon surface uses anisotropic wet chemical etching (e.g., KOH) to produce randomly distributed pyramidal pits,[10-13] patterned, for example, using etch masks of randomly dispersed colloids.[13] Experimental studies of this approach show that interaction length enhancements of up to 12 times are possible[14] for wavelengths near 1 μm in thin films of silicon. Alternatively, photolithography and etching can form structures of relief with excellent levels of engineering control over the geometries.[15-17] Recent work shows that periodic gratings as photonic crystal back reflectors on ~5 μm thick layers of silicon derived from silicon-on-insulator (SOI) wafers enable ~15% increases in energy conversion efficiency compared to similar cells without back reflectors.[18,19] Although useful for exploring the physics, these types of cells rely on high cost materials and processing methods. A different approach uses vertically aligned silicon wires combined with ARCs, backside reflectors, and embedded particles for light scattering to achieve absorption greater than 80%, for a volume of silicon equivalent to a uniform film with thickness of 3 μm. This result corresponds to a ~140% improvement over the case of the bare film.[20] These wire-based structures have not yet, however, been used to create working devices whose performance can be evaluated and benchmarked against alternatives.

In the following, we describe the use of soft imprint lithography to generate submicrometer, periodic features of relief as light trapping structures (LTS) on thin, monocrystalline silicon solar cells derived from bulk wafers. These procedures and cells have characteristics that give them some potential for practical use, especially in applications where thin, small geometries provide unique advantages. Simulations based on rigorous coupled wave analysis (RCWA) and finite difference time domain (FDTD) methods, supported by experimental measurements, yield guidelines for design choices and insights into important optical effects, including reflection, diffraction, and light trapping. We begin by describing the fabrication procedures, and then outlining experimental and simulation studies of the optics. We conclude with demonstrations on working solar cells and comparisons to control samples.

For modules, we used arrays of ultrathin, monocrystalline silicon solar cells (i.e., microcells) with widths of 50 μm, lengths of 1.55 mm, and thicknesses (t) of ~6 μm, fabricated from p-type ⟨111⟩ Czochralski Si wafers (1−10 Ω cm,

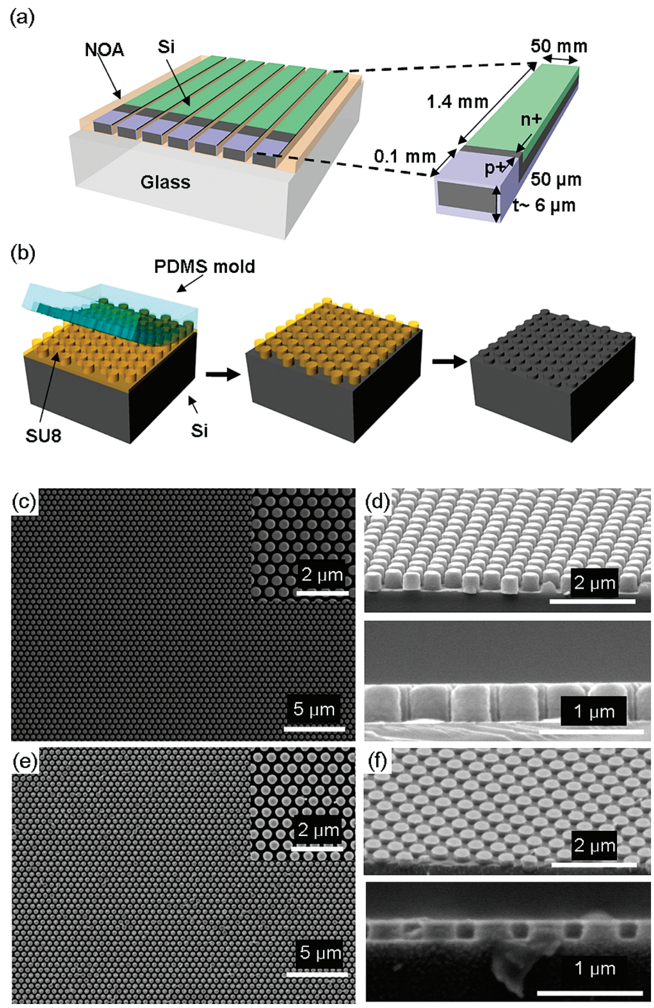

FIGURE 1. Schematic illustrations and scanning electron micrographs (SEMs) of silicon microcell devices and fabrication procedures. (a) Diagram of a module (left) that incorporates interconnected arrays of microcells (right). The doping profiles for a top contact layout appear in color (green for n-type doping, blue for p-type doping). (b) Process for forming light-trapping structures (LTS) on the top surface of a microcell. (c) and (d) Top, angled, and cross sectional SEMs of polymer nanostructures formed by soft imprint lithography. (e) and (f) Top, angled, and cross sectional SEMs of silicon nanostructures formed by etching.

Virginia Semiconductor), printed in arrays onto glass substrates (~1 mm thickness) using procedures described in detail elsewhere.[4] Figure 1a illustrates schematically a representative module and an individual microcell, with a doping profile designed for top contacts to p and n regions. Figure 1b outlines the process for forming an LTS consisting of posts of silicon on the top surfaces of the microcells in this type of module. The first step involves spin coating a uniform, ~200 nm thick layer of epoxy (SU8, MicroChem, Inc., 4 wt % in cyclopentenone, 3000 rpm for 30s) onto the module surface. Soft nanoimprint lithography (95 °C for 3 min) forms submicrometer, periodic features of relief on the surface of this layer. Reactive ion etching (RIE) (10 sccm, 50 mTorr, and 45 s) with oxygen removes the residual material at the base of

DOI: 10.1021/nl101510q | *Nano Lett.* **2010,** *10,* 3041--3046

the recessed features. The remaining posts serve as a mask for selective removal of silicon by inductively coupled plasma reactive ion etching (SF_6 50 sccm, C_4F_8, 80 sccm, O_2, 5 sccm). Immersion in pirahna solution (3:1 ratio of H_2SO_4 and H_2O_2) for 30 s eliminates the remaining polymer to complete the fabrication. Parts c and d of Figure 1 provide top, side, and angled view scanning electron micrographs of a thin epoxy layer molded into a hexagonal array of posts with a periodicity (P) of 500 nm, relief depth (RD) of 400 nm, and post diameter (D) of 370 nm. The underlayer here is approximately ~50 nm thick. The processing steps outlined above yield corresponding silicon structures, with similar geometries, i.e., RD =130 nm and D = 360 nm. The uniformity over large areas is good, as shown in Figure 1e (top view) and Figure 1f (side and angled views). The depth of relief in the silicon can be controlled precisely by adjusting the time for etching.

Such LTS can enhance absorption by (i) reducing reflections at the front surface, (ii) increasing the optical path length through diffraction, and (iii) trapping higher order diffracted light due to total internal reflection (TIR). The structure of the LTS, therefore, should be selected to minimize reflections and maximize diffraction, particularly into orders at sufficiently steep angles to yield TIR. On the basis of these considerations, we fabricated LTS of silicon posts with P = 500 nm, RD = 130 nm, and D = 350 nm. Detailed exploration of other geometries by FDTD and RCWA modeling appears in a following section. Figure 2 shows measured and simulated transmission, reflection, and inferred absorption spectra for functional microcells (6 μm thick), consisting of bare silicon, silicon with a single layer ARC (80 nm SiO_2; ARC), with an LTS (P of 500 nm; LTS), and with both an LTS and an ARC (LTS+ARC). The measurements used an optical microscope (Carl Zeiss, Inc., Axio Observer D1, 20× objectives with an NA of 0.46) coupled to a fiber-optic spectrometer (Control Development, Inc.). (We applied a smoothing filter to the measured data to reduce noise and facilitate comparison to simulation. Raw data from 350 to 1050 nm can be found in Supporting Information.) Simulations in this case used FDTD, with literature values for the optical properties of the silicon[21,22] and with cells that extend infinitely in the $x-y$ plane and have some thickness in the z direction. For simplicity, changes in these properties due to patterned doping profiles (Figure 1a) and other aspects of processing (i.e., roughened sidewall and back surfaces; finite lateral extent) were not included. As shown in Figure 2a, microcells with an LTS and with an ARC both have significantly reduced reflection compared to bare silicon. The LTS+ARC case provides the lowest reflection throughout the spectral range, consistent with simulation results in Figure 2b. Figure 2c indicates that the ARC case has the highest transmission, as might be expected. The LTS and LTS+ARC exhibit lower transmission compared to bare silicon, consistent with their ability to increase the optical path length via diffraction and trapping. The simulation results of Figure 2d show good agreement with these measurements. Figure 2e presents absorption (i.e., 100% − R − T) spectra for these same cells. As expected, the cases of bare silicon and LTS+ARC show the lowest and highest absorption, respectively, in agreement with simulation results in Figure 2f. The absorption integrated over the wavelength range of 450 to 1000 nm and weighted by the solar radiation spectrum (Air Mass 1.5D) for LTS+ARC, LTS, ARC, and bare silicon are 84%, 83%, 56%, and 45%, respectively. The values for the LTS+ARC are comparable to the silicon wire approach mentioned previously.[20] Devices with thicknesses of 3 μm and backside reflectors provide a more direct comparison; simulations for this case show behavior similar to the 6 μm thick cells (without backside reflectors) described here.

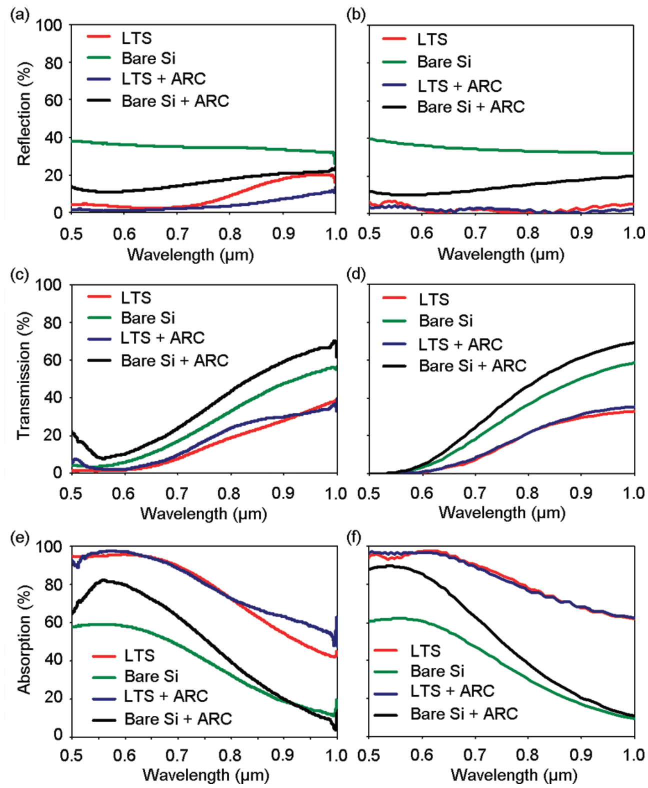

FIGURE 2. Experimentally measured and simulated transmission (a) and (b), reflection (c) and (d), and absorption (e) and (f) spectra for light normally incident on silicon microcells with thicknesses of 6 μm. Four types of cells were examined: bare silicon, ARC, LTS, and LTS+ARC.

The experimental results of Figure 2 validate the modeling approaches, thereby justifying their use in exploring other LTS geometries. To this end, we performed systematic simulations with both FDTD and RCWA techniques on slabs of silicon with thicknesses of 6 μm and hexagonal arrays of posts with and without a layer of SiO_2 (~80 nm) as an ARC. Figure 3a summarizes results for absorption of normally incident standard solar radiation (Air Mass 1.5D), over a spectral range from 350 to 950 nm, with a 10 nm simulation

DOI: 10.1021/nl101510q | Nano Lett. 2010, 10, 3041–3046

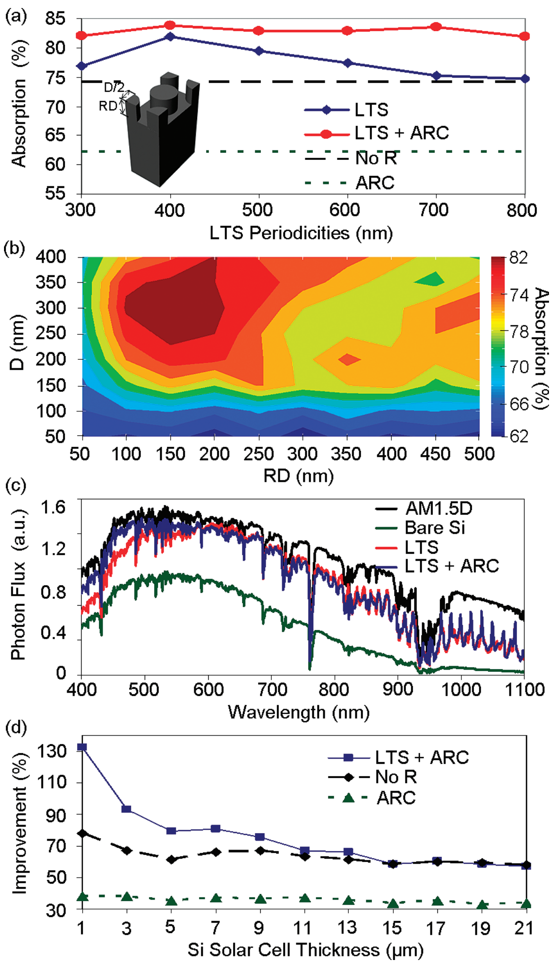

FIGURE 3. Comparative studies of absorption in slabs of silicon with different surface preparations, by RCWA and FDTD modeling. (a) Calculated absorption averaged over the solar spectrum for LTS with different periodicities and a silicon thickness of 6 μm. Bare silicon with no reflection (No *R*) and bare silicon with ARC (ARC) are included for comparison. The inset shows the geometry of a unit cell. (b) Contour map of calculated absorption as a function post diameter (*D*) and relief depth (RD). (c) Simulation of photon flux absorbed for illumination by the AM 1.5D reference spectrum (also shown) as a function of wavelength for bare silicon, LTS, and LTS+ARC. (d) Calculated percent improvement in integrated absorption of AM1.5D radiation for LTS+ARC, No *R*, and ARC, compared to bare silicon as a function of solar cell thickness.

step size, for several different cases. The inset shows the unit cell geometry. Bare silicon absorbs approximately 45% of the solar radiation. This absorption increases to 62% with the addition of an ARC (SiO_2; 80 nm). For an ideal case (i.e., perfect ARC), where the reflection is zero, the absorption is 74%. For all values of P investigated, LTS provides improved absorption compared to this no reflection case. The relative percentage improvements over bare silicon and single layer ARC for $P = 300$, 400, 500, 600, 700, and 800 nm are 72% and 24%, 83% and 32%, 78% and 28%, 73% and 25%, 68% and 21%, and 67% and 20%, respectively. The LTS+ARC further increases the absorption, with $P = 400$ nm providing the highest value (84%), corresponding to an 88% and 35% improvement over bare silicon and ARC, respectively. The calculated absorption also agrees with that measured from optical spectra (Figure 2). Tables summarizing simulation results can be found in Supporting Information (Table S1). The values of RD and *D*, for a given *P*, are critically important because they determine the distribution of intensity into the diffraction orders. Figure 3b provides a contour map of the absorption as a function of *D* (*y* axis) and RD (*x* axis), for the case of a 6 μm thick layer of silicon with LTS+ARC and $P = 500$ nm. The absorption varies through this range by ~20% (i.e., from 82% to 62%). The highest values occur between 100 to 200 nm and 200 to 400 nm for RD and *D*, respectively. This range of RDs provides low reflection loss through the range of wavelengths where solar radiation is the strongest; these same parameters provide relatively low reflection throughout the entire spectrum. The optimal range of *D* maximizes the distribution of light into diffraction orders; substantially lower or higher values lead to weak diffraction. To provide additional insights, Figure 3c presents the absorption of the entire solar spectrum for the cases of bare silicon, LTS, and LTS+ARC with *P* of 500 nm, *D* of 360 nm, and RD of 130 nm. The results show that the addition of an ARC to the LTS structure offers benefits mainly in the short wavelength range.

As expected, the thickness of the silicon determines the level of improvement provided by the LTS. For example, the LTS cannot outperform an optimized ARC for bulk devices. Figure 3d shows the thickness dependence of the percent improvement in absorption, compared to bare silicon, for LTS+ARC (*P* of 500 nm, RD of 150 nm, and *D* of 350 nm), ARC, and bare silicon with no reflection. These results indicate that the LTS+ARC increases the absorption beyond levels possible with no reflection when the thickness is less than ~10 μm. In the limit of large thicknesses, the LTS+ARC performs almost as well as the no reflection case. As the thickness of the silicon increases, the dominant effect shifts from light trapping to antireflection. Improvement with the ARC is ~35% throughout this thickness range, indicating a fairly constant reflection loss. Tables summarizing simulation results in Figure 3d can be found in Supporting Information (Table S2).

The increase in absorption translates directly into an increase in the energy conversion efficiency. Figure 4 shows representative current density (*J*)−voltage (*V*) measurements of a single, individual microcell prepared in different configurations and measured using a simulated AM 1.5D illumination of 1000 W/m^2 at room temperature, on a black anodized metal surface to suppress reflections. Several cases were examined, sequentially, with this cell: bare silicon, bare silicon with an ARC, with LTS, and with LTS+ARC, where short circuit current densities (J_{sc}) were found to be 14.9, 18.3, 24.0, and 35.5 mA/cm^2, open circuit voltages (V_{oc}) were 0.49, 0.51, 0.51, and 0.52 V, fill factors, FF, were 0.72, 0.73, 0.71, and 0.70, and efficiencies (η) were 5.2, 6.8, 8.7, and 9.5%, respectively. (The calculated efficiencies use the

DOI: 10.1021/nl101510q | *Nano Lett.* **2010,** *10,* 3041–3046

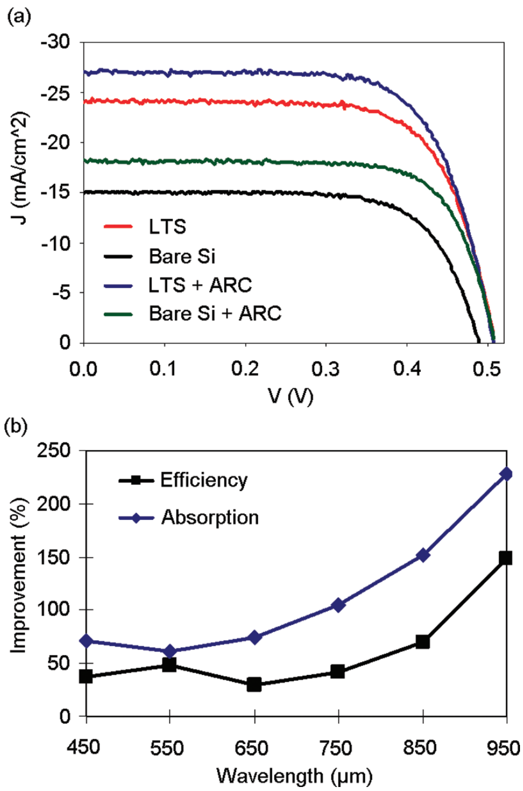

FIGURE 4. Measurements of energy conversion efficiency in silicon microcells. (a) $J-V$ curves for microcells consisting of bare silicon, bare silicon with ARC, LTS, and LTS+ARC, under AM 1.5D illumination. (b) Spectrally resolved improvements in efficiency and absorption for microcells with LTS compared to those with bare silicon. The improvements correspond to the difference between values measured with LTS and those with bare silicon, divided by the value for bare silicon, times 100%.

top surface areas of the devices rather than the areas of the p−n junctions.) Electrical measurements for bare silicon, LTS, and LTS+ARC were performed on the same silicon cell after each processing step. Tables summarizing electrical measurements can be found in Supporting Information (Table S3). The electrical measurements for bare silicon cell with ARC were measured after all processing steps on the silicon cell positioned right next to the silicon cell for other measurements, to avoid any effects associated with cell-to-cell, position related variations within the module. Standard deviations in measured values of η, V_{oc}, and FF for typical silicon cells (15 μm thick, η of 6.7%, V_{oc} of 0.485 V, FF of 0.7) fabricated in the same batch are 0.44%, 0.006 V, 0.01, respectively. We did not observe degradation in any of these properties due to the fabrication steps. The LTS+ARC achieves the highest overall efficiency, corresponding to an 83%, 40%, and 9% increase compared to bare silicon, ARC, and LTS cases, respectively. The results of Figure 4a are similar to those obtained from simulations (Figure 3a): 85%, 33%, and 5%, respectively. Figure 4b shows relative improvements in efficiency and absorption, measured at different wavelengths by insertion of narrow band filters in front of the solar simulator, for bare cells and those with LTS. Tables summarizing spectral resolved efficiency and absorption measurements can be found in the Supporting Information (Table S4.) Both parameters exhibit similar trends, with larger increases at longer wavelengths, where the silicon absorption decreases and the effect of light trapping increases. The improvement reaches its peak at 950 nm and reduces again at 1050 nm, due to the very weak absorption of silicon in this region.

To summarize, nanostructures of relief formed by molding and etching the surfaces of silicon microcells can improve their performance significantly at thicknesses less than ∼10 μm, due to diffractive and trapping effects that improve the absorption by increasing the optical path length. The significance of this result is not only that it offers the opportunity to reduce the usage of silicon but also that it facilitates and enhances many of the characteristics that create interest in this microcell technology. As examples, decreasing the thickness decreases the weight, increases the bendability (in flexible designs), and improves the radiation resistance. These outcomes and the more general design considerations reported here might be useful for future work in silicon and other classes of photovoltaic systems, particularly in ultrathin designs.

Acknowledgment. This work was financially supported by the Department of Energy award DE-FG02-07ER46471, through the Materials Research Laboratory (MRL), and by an Energy Frontier Research Center. The manufacturing and fabrication aspects were funded by the National Science Foundation (DMI-0328162).

Note Added after ASAP Publication. This paper published ASAP June 28, 2010 with errors in the second, sixth, and seventh paragraphs. The correct version published on June 30, 2010.

Supporting Information Available. Reflection, transmission, and absorption spectra and tables showing absorption improvement compared to bare silicon and electrical characterization of an individual silicon microcell. This material is available free of charge via the Internet at http://pubs.acs.org.

REFERENCES AND NOTES

(1) Bagnall, D. M.; Boreland, M. *Energy Policy* **2008**, *36*, 4390.
(2) Minemoto, T.; Takakura, H. *Jpn. J. Appl. Phys.* **2007**, *46*, 4016.
(3) Verlinden, P. J.; Blakers, A. W.; Weber, K. J.; Babaei, J.; Everett, V.; Kerr, M. J.; Stuckings, M. F.; Gordeev, D.; Stocks, M. J. *Sol. Energy Mater. Sol. Cells* **2006**, *90*, 3422–3430.
(4) Yoon, J.; Baca, A. J.; Park, S.-I.; Elvikis, P.; Geddes, J. B.; Li, L.; Kim, R. H.; Xiao, J.; Wang, S.; Kim, T. H.; Motala, M. J.; Ahn, B. Y.; Duoss, E. B.; Lewis, J. A.; Nuzzo, R. G.; Ferreira, P. M.; Huang, Y.; Rockett, A.; Rogers, J. A. *Nat. Mater.* **2008**, *7*, 907–915.
(5) Mack, S.; Meitl, M. A.; Baca, A. J.; Zhu, Z. T.; Rogers, J. A. *Appl. Phys. Lett.* **2006**, *88*, 213101.
(6) Ko, H. C.; Baca, A. J.; Rogers, J. A. *Nano Lett.* **2006**, *6*, 2318.
(7) Ahn, B. Y.; Duoss, E. B.; Motala, M. J.; Guo, X.; Park, S.-I.; Xiong, Y.; Yoon, J.; Nuzzo, R. G.; Rogers, J. A.; Lewis, J. A. *Science* **2009**, *323*, 1590.

(8) Baca, A. J.; Yu, K. J.; Xiao, J.; Wang, S.; Yoon, J.; Ryu, J. H.; Stevenson, D.; Nuzzo, R. G.; Rockett, A. A.; Huang, Y.; Rogers, J. A. *Energy Environ. Sci.* **2010**, *3*, 208.
(9) Yablonovitch, E. *J. Opt. Soc. Am.* **1982**, *72*, 899.
(10) Campbell, P.; Green, M. A. *J. Appl. Phys.* **1987**, *62*, 243.
(11) Kim, K.; Dhungel, S. K.; Jung, S.; Mangalaraj, D.; Yi, J. *Sol. Energy Mater. Sol. Cells* **2008**, *92*, 960.
(12) Smith, A. W.; Rohatgi, A. *Sol. Energy Mater. Sol. Cells* **1993**, *29*, 37.
(13) Deckman, H. W.; Dunsmuir, J. H. *Appl. Phys. Lett.* **1982**, *41*, 37.
(14) Deckman, H. W.; Roxlo, C. B.; Yablonovitch, E. *Opt. Lett.* **1983**, *8*, 491.
(15) Gale, M.; Curtis, B.; Kiess, H.; Morf, R. H. *Proc. SPIE* **1990**, *1272*, 60.
(16) Heine, C.; Morf, R. H. *Appl. Opt.* **1995**, *34*, 2476.
(17) Eisele, C.; Nebel, C.; Stutzmann, M. *J. Appl. Phys.* **2001**, *89*, 7722.
(18) Zeng, L.; Yi, Y.; Hong, C.-Y.; Liu, J.; Feng, N.; Duan, X.; Kimerling, L. C.; Alamariu, B. *Appl. Phys. Lett.* **2006**, *89*, 111.
(19) Zeng, L.; Bermel, P.; Yi, Y.; Alamariu, B. A.; Broderick, K. A.; Liu, J.; Hong, C.; Duan, X.; Joannopoulos, J.; Kimerling, L. C. *Appl. Phys. Lett.* **2008**, *93*, 221105.
(20) Kelzenberg, M. D.; Boettcher, S. W.; Petykiewicz, J. A.; Turner-Evans, D. B.; Putnam, M. C.; Warren, E. L.; Spurgeon, J. M.; Briggs, R. M.; Lewis, N. S.; Atwater, H. A. *Nat. Mater.* **2010**, *9*, 368.
(21) Hull, R. *EMIS Data Reviews Series No 20*, INSPEC, London, 1999, p 677.
(22) Globus, T.; Jones, S. H.; Digges, T. *Proc.— Int. Semicond. Device Res. Symp., 1997* **1998**.

DOI: 10.1021/nl101510q | *Nano Lett.* **2010,** *10,* 3041--3046